Transition to chaos by interaction of resonances in dissipative systems. II. Josephson junctions, charge-density waves, and standard maps

Tomas Bohr
Laboratory of Atomic and Solid State Physics, Cornell University, Ithaca, New York 14853

Per Bak
Physics Department, Brookhaven National Laboratory, Upton, New York 11973

Mogens Høgh Jensen
H. C. Ørsted Institute, Universitetsparken 5, DK-2100 Copenhagen Ø, Denmark
(Received 9 May 1984)

We have studied the transition to chaos caused by interaction and overlap of resonances in some condensed-matter systems by constructing and analyzing appropriate return maps. In particular, the resistively shunted Josephson junction in microwave fields and charge-density waves in rf electric fields may be described by the differential equation of the damped driven pendulum in a periodic force. The two-dimensional return map for this equation is shown to collapse to a one-dimensional circle map in a parameter regime including the transition to chaos. Phase locking, noise, and hysteresis in these systems can thus be understood in a simple and coherent way by taking over theoretical results for the circle map, some of which were derived in the preceding paper. In order to understand the contraction to one dimensionality we have studied the two-dimensional Chirikov standard map with dissipation. A well-defined transition line along which the system exhibits circle-map critical behavior was found. At this line the system is always phase locked. We conclude that recent theoretical results on universal behavior can readily be checked experimentally by studying systems in condensed-matter physics. The relation between theory and experiment is simple and direct.

I. INTRODUCTION

The purpose of this paper is to demonstrate that there exist some simple condensed-matter systems which exhibit a transition to chaos caused by overlap of resonances with universal critical behavior as described in the preceding paper. Differential equations for the dynamics of these systems can be represented by one- and two-dimensional discrete maps, permitting direct confrontation of recent theories with experiment, and providing an understanding of phase locking, hysteresis, and noise phenomena which have been observed.

In the 17th century Christiaan Huyghens noted that two clocks hanging back to back on the wall tend to synchronize their motion.[1] More generally, strongly coupled damped oscillators tend to lock into commensurate motion where the ratio of their frequencies is a rational number. This phenomenon is known as phase locking and it is generally present in dissipative dynamical systems with competing frequencies. The two frequencies might arise dynamically within the system (as Huyghens's coupled clocks) or through the coupling of an oscillating or rotating motion to an external periodic force—as in a "swing." In many-dimensional systems the effective loss of degrees of freedom through dissipation may reduce the phase-locking phenomenon to basically two coupled oscillators.

If some parameter is varied, the system may pass through regimes which are phase locked and regimes which are not. For weakly nonlinear coupling the phase-locked intervals will have small measure. The motion is either (with small probability) periodic or, more likely, quasiperiodic, i.e., the ratio between the two frequencies ω_1/ω_2 is irrational. As the nonlinearity increases, the phase-locked portions increase and chaotic motion may occur in addition to the periodic and quasiperiodic (incommensurate) motion. The onset of chaos is basically caused by the growth of the phase-locked intervals until they eventually overlap, causing hysteretic response as well as truly chaotic behavior.

In the preceding paper (I) we gave strong numerical evidence for universal scaling behavior of the phase-locked steps on the critical line of the one-dimensional (1D) circle map. We shall here give evidence that the *same* scaling behavior should be found for the dissipative phase-locked systems described above. In particular, the theory applies to the resistively shunted Josephson junction in a microwave field, and sliding charge-density waves (CDW) in rf electric fields. The return maps for these systems are two-dimensional maps which collapse to 1D because of the dissipation. A short account of some of our results has already been published.[2]

For the circle maps studied in I the critical line is just $K=1$, but for higher-dimensional systems no such simple relation exists in general. We shall present evidence, however, derived from a two-dimensional dissipative map that a "critical line" does exist where the measure of the

phase-locked intervals is 1 and above which the intervals start to overlap. Most importantly, this line seems to be a continuous function of the parameters in the sense that the high-order mode-locked intervals determine a smooth critical curve (see Fig. 1). Along this line the complement to the locked portions is a measure-0 Cantor set, and we find the fractal (or Hausdorff) dimension of the set to be the same universal number $D \sim 0.87$ as found for the circle map.

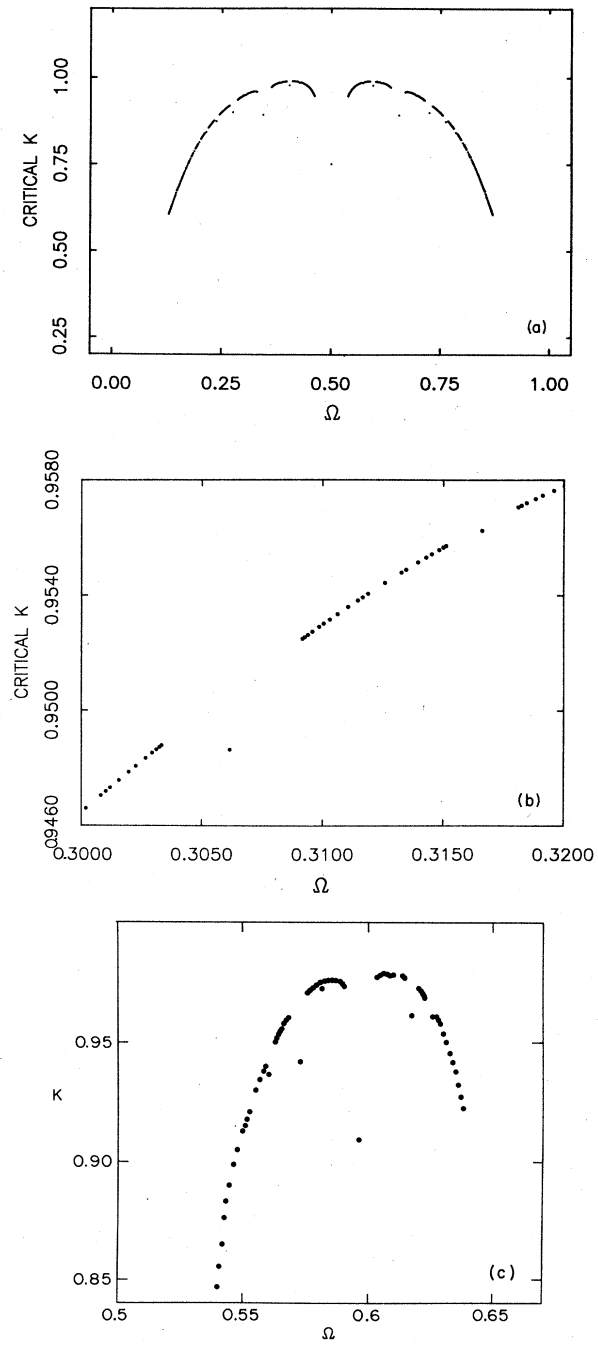

FIG. 1. Critical curves for 2D standard map with dissipation, calculated as discussed in Sec. V. (a) The curve was calculated for $b=0.25$; (b) the curve is a magnification g of (a); (c) the curve was calculated for $b=0.5$, $\frac{1}{2} < W < \frac{2}{3}$.

Schematically, the connection between the physical system and the circle map can be represented as follows:

Physical system

(pendulum, CDW, Josephson junction)

↕

Differential equation

↕

2D discrete return map

↕

1D circle map (universal behavior)

The physical system is described by a differential equation; the return map for the differential equation is a two-dimensional (2D) discrete map; finally, the 2D return map collapses to a 1D circle map exhibiting universal behavior, i.e., there exists a 1D invariant curve.

The close resemblance between real coupled oscillator systems and the one-dimensional circle maps which we are suggesting might—from a mathematical viewpoint—seem to be a strange result. For the one-dimensional maps there exist strong theorems[3] guaranteeing that any monotonic, smooth map exhibits only periodic or quasiperiodic behavior. On the other hand, for higher-dimensional maps the analog [Komolgorov-Arnol'd-Moser (KAM) -like] theorems[4] only prove the existence of quasiperiodic motion (invariant tori) for maps that are "sufficiently close" to the trivial ones and no simple criterion for the breakdown of tori exists.

What we find here is the following: If, instead of looking at the original two-dimensional map, we project out the angular variable and consider the corresponding one-dimensional map (termed the "reduced map" in Sec. III), the criterion for having smooth invariant tori is—just as for the circle-map case—that this map be monotonic. Of course, we do not in general know where the monotonicity breaks down in terms of the parameters of the original map, but it does tell us that the situation, in terms of renormalized parameters, is very close to the 1D case.

The layout of this paper is as follows. In Sec. II we shall discuss the Josephson junction in microwave fields and sliding CDW's (as found, for instance, in niobium triselenides, $NbSe_3$) in applied dc plus ac electric fields. These systems are described by the differential equation for a damped pendulum driven by a constant plus a periodic torque—so, in principle, our results can be tested on this simple mechanical device. We hope that experiments on Josephson junctions and CDW's be performed since they can be done with great precision.

In Sec. III we discuss general properties of return map for dissipative dynamical systems. We show numerically that the 2D return map of the equation for the Josephson junction reduces to a 1D map.

In Sec. IV we shall discuss in general the "criticality" for a 2D map which collapses to a 1D circle map, taking as the basic definition that the map becomes critical when the smooth invariant curve disappears.

As a concrete example we shall study a particular 2D

map, the "Chirikov standard map with dissipation" in Sec. V. We present numerical evidence that the critical line is smooth and that there is scaling behavior of the mode-locked intervals as for the circle map.

II. PHASE LOCKING IN JOSEPHSON JUNCTIONS AND CDW SYSTEMS

Phase locking is basically a resonance effect between two oscillators. Even simpler, one can consider systems where one of the oscillators is replaced by an external perturbation; this also facilitates quantitative measurements of high-order locked motion since one of the frequencies is given as a parameter. The ubiquitous differential equation

$$\alpha\ddot{\theta}+\beta\dot{\theta}+\gamma\sin\theta=A+B\cos\omega t \tag{2.1}$$

is precisely of this form. It describes a periodically forced, damped pendulum, with mass α, damping coefficient β, and gravitational field γ. The equation is also—among other things—believed to give a fair description of a Josephson junction when the current has both a super and a normal part, and of sliding CDW's in electric fields.

It should be emphasized at this point that the precise form of (2.1) is immaterial for our investigation. Our aim is to find universal properties which should be independent of additional nonlinear terms in the equation, substitution of other periodic functions for $\sin\theta$, etc. We have chosen (2.1) as the simplest form to capture the essential physics. Figure 2 shows the equivalent electric diagram for the Josephson junction. Here, θ is the phase difference across the junction, and it is seen that $\alpha=\hbar C/2e$, $\beta=\hbar/2eR$, and γ is the critical current I_c. Finally, A and B are the amplitudes of the dc and ac microwave components of the current through the junction. This model is usually referred to as the resistively shunted Josephson junction (RSJ) model, and a vast literature exists about it.[5] For certain values of the parameters the junction can be driven to a noisy state,[6,7] and indeed numerical simulations have indicated that the noise arises as chaotic solutions to the differential equation.[8–10] A sequence of bifurcations leading to chaotic behavior is known in a qualitative way from Refs. 7 and 11.

In the CDW systems, θ is the position of a sliding

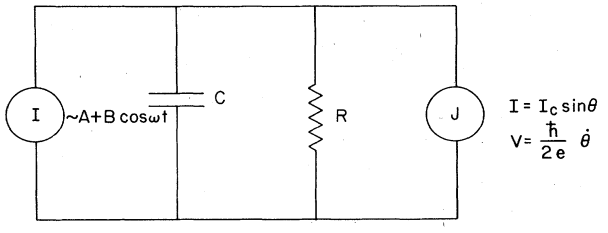

$$A+B\cos\omega t = C\frac{dV}{dt}+\frac{V}{R}+I_c\sin\theta$$
$$= \frac{\hbar C}{2e}\ddot{\theta}+\frac{\hbar}{2eR}\dot{\theta}+I_c\sin\theta$$

FIG. 2. Diagram for the resistively shunted Josephson junction, driven by a constant current A and a microwave current with amplitude B.

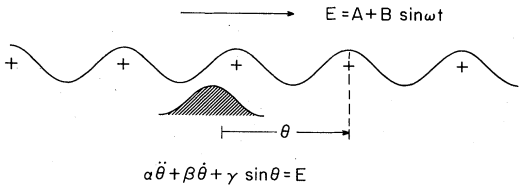

FIG. 3. Sliding charge density wave in ac plus dc electric field, and a quenched impurity pinning potential. For a single-domain sample the pinning potential could be a contact potential. The motion is that of a particle rolling down an oscillating washboard.

CDW relative to an "impurity" pinning potential (Fig. 3). For a single-domain sample, the pinning potential is probably a contact potential. The parameters α, β, and γ are phenomenological parameters representing the effective mass, damping, and periodic potential.[12,13] A is a dc electric field which depins the CDW when it exceeds a critical value, and B is the amplitude of an oscillating rf electric field.

In those systems the phase-locking phenomenon shows up as tendency of the average (angular) velocity $\langle\dot{\theta}\rangle$ to lock into rational multiples of the frequency of the external field,

$$\langle\dot{\theta}\rangle=\frac{P}{Q}\omega\ . \tag{2.2}$$

Why does this mode locking occur? For small torque A on the pendulum (or dc current in the Josephson junction, or dc voltage in the CDW system) the pendulum stays near its downward position. When A exceeds a critical value, the pendulum enters a running "rotating" mode with average velocity $\sim A/\beta$ (for γ and B not too large).

Due to the periodicity of $\gamma\sin\theta$ and $B\cos\omega t$ the configuration space (θ,t) should really be thought of as a periodic lattice on which the motion takes place as shown in

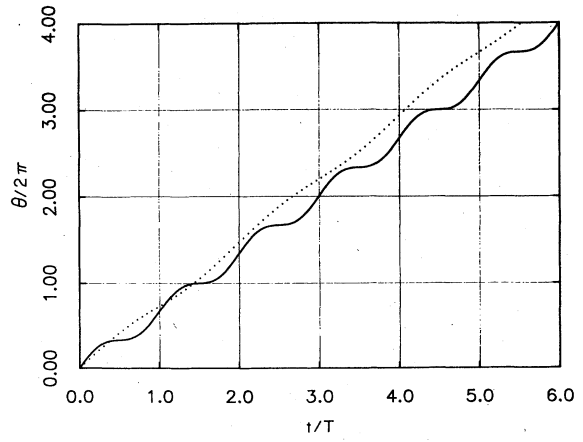

FIG. 4. Phase versus time for rotating pendulum, for a torque A (or dc current I in the Josephson junction or dc field E in the CDW systems) exceeding the critical value. The time is measured in units of $2\pi/\omega$, i.e., the external force is used as a clock. The dotted curve indicates quasiperiodic motion, the solid curve periodic motion.

Fig. 4. Alternatively, one can pick out a rectangle of this lattice and identify opposite sides, thereby obtaining a two-dimensional torus which then forms the configuration space for the equation (Fig. 5). The dotted motion in Fig. 4 is quasiperiodic or incommensurate because its periodicity is unrelated to the underlying lattice, and on the torus the orbit would be dense and never close on itself. When the nonlinearities γ and B become large there will be a more pronounced tendency of the motion to fit into the lattice (as for the commensurate-incommensurate transition in adsorbed monolayers, etc.[15]) as shown by the solid curve. Here there exist integer numbers N and M such that

$$\theta(t_0+MT)=\theta(t_0)+2\pi N \tag{2.3}$$

or

$$\langle\dot{\theta}\rangle=\frac{N}{M}\frac{2\pi}{T}=\frac{N}{M}\omega\ , \tag{2.4}$$

where T is the "clock" period of the external force.

If the situation (2.3) is realized for a certain parameter value (for instance a value of A), then there always exist an entire interval around this value where (2.4) is satisfied for the same N and M; we have phase locking.

The above argument merely makes it plausible that locking might occur, and it would seemingly work just as well for $\alpha=0$, the zero mass, or overdamped case, where the model reduces to the Stewart-McCumber[16] model. In fact, it has been shown rigorously that in this limit only the whole multiples ($M=1$) of ω survive since (2.1) is then a linear equation (the Mathieu equation) in disguise.[17] The coefficient of the $\ddot{\theta}$ term is thus a measure of the nonlinearity of the system.[18]

For the Josephson junction the voltage V is given by the Josephson relation

$$V=\frac{\hbar}{2e}\dot{\theta}\ , \tag{2.5}$$

so a locking of $\langle\dot{\theta}\rangle$ implies a locking of $\langle V\rangle$ and steps will be seen in the I-V characteristics. For $M=1$ these are the Shapiro steps,[19] but in between them subharmonic steps (with $M>1$) can often be seen.[20] Figure 6 shows the striking experimental observation by Belykh *et al.*[7] of a multitude of such substeps in the I-V characteristics of a Nb-Nb Josephson junction.

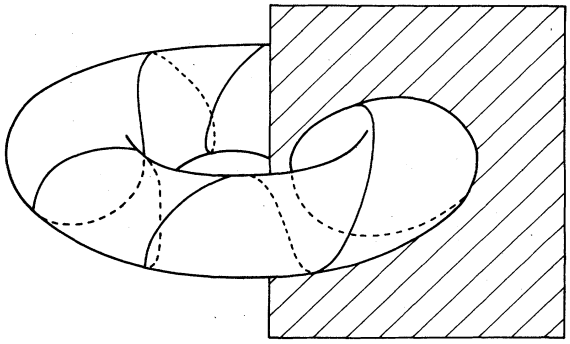

FIG. 5. The configuration space as the surface of a 2D torus. A possible orbit is indicated on the torus, and a plane with constant t mod$2\pi/\omega$ is shown, on which the return map is generated.

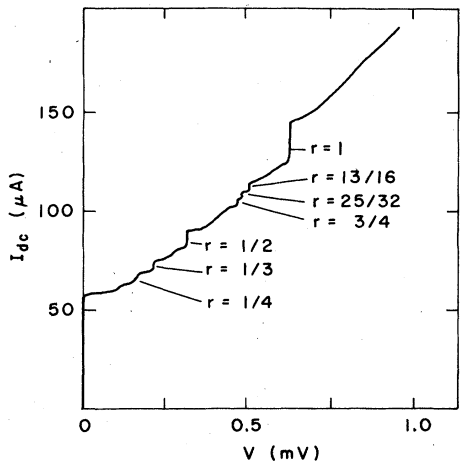

FIG. 6. I-V characteristics of an *NB-Nb* Josephson point junction in 295 GHz microwave field at $T=4.2$ K. (Belykh, Pedersen, and Soerensen, Ref. 7.)

In the CDW systems the current carried by the sliding charge-density wave is proportional to the velocity $\dot{\theta}$, so the average current is

$$I_{\mathrm{CDW}}\sim\langle\dot{\theta}\rangle\ . \tag{2.6}$$

Hence, a locking of $\langle\dot{\theta}\rangle$ implies a locking of the current carried by the CDW (the current carried by the normal electrons behaves in a smooth way, $I_n\sim E$). The roles of currents and voltages are the reverse for Josephson junctions and CDW systems.

It has been suggested that the mass α of the CDW systems is essentially zero, so there would be essentially no subharmonic steps in apparent agreement with early measurements.[13,14] Recently, however, a multitude of such steps have been observed in a striking experiment by Brown, Mozurkewich, and Grüner;[21] the situations for CDW systems and Josephson junctions seem to be essentially the same.

III. THE RETURN MAP

The most effective way of studying phase locking of differential equations such as (2.1) is through their return maps, i.e., the mapping of the variables θ and $\dot{\theta}$ at the beginning of the nth period $T=2\pi/\omega$ to the values of the variables at the end of that period. In Fig. 5 a plane with $t=$const (mod $2\pi/\omega$) is shown and the return map R is

$$\underline{R}\begin{bmatrix}\theta_n\\ \dot{\theta}_n\end{bmatrix}=\begin{bmatrix}\theta_{n+1}\\ \dot{\theta}_{n+1}\end{bmatrix}=\begin{bmatrix}G_1(\theta_n,\dot{\theta}_n)\\ G_2(\theta_n,\dot{\theta}_n)\end{bmatrix}\ , \tag{3.1}$$

where $(\theta_n,\dot{\theta}_n)=(\theta(t=nT),\ \dot{\theta}(t=nT))$. Since the differential equation is of second order, the two variables θ_n and $\dot{\theta}_n$ contain all information about the system at a given time; therefore, the return map is two dimensional.

The functions G_1 and G_2 must be periodic in θ with

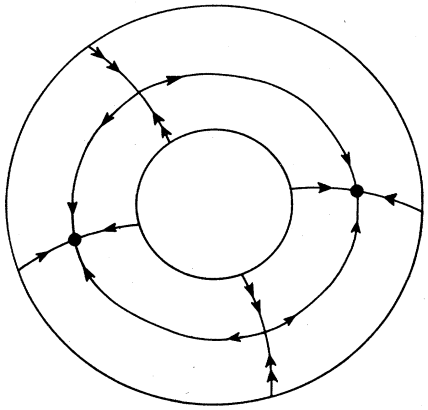

FIG. 7. Annular map (schematic) showing the invariant circle and the invariant manifolds. The simplest locked state is shown with a stable and unstable fixed point.

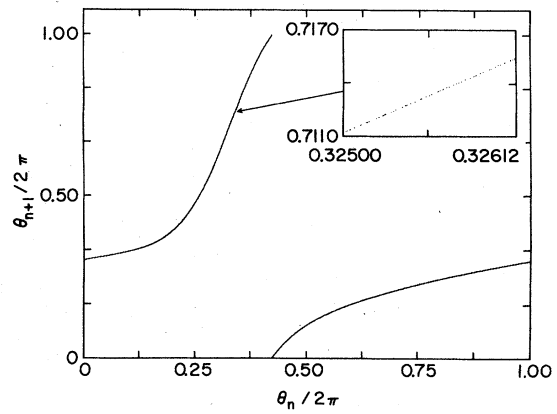

FIG. 8. Return map calculated for $B=\alpha=\gamma=1$, $\omega=1.76$, $\beta=1.576$, $A=1.4$. The function $f(\theta_n)=\theta_{n+1}$ is monotonically increasing indicating regular behavior. The inset is a magnification, emphasizing the one dimensionality of the map.

period 2π since that period is explicit in (2.1). Thus the map R can be thought of either as mapping the plane into itself, or—identifying θ values differing only by multiples of 2π—as a mapping of a cylinder (or an annulus) to itself, as shown in Fig. 7.

Since the points $(\theta_n,\dot{\theta}_n)$ are points on a solution curve for a differential equation, the map must be invertible and orientation preserving. This means that the Jacobian

$$J=J(\theta_n,\dot{\theta}_n)=\det\begin{bmatrix}\frac{\partial G_1}{\partial\theta_n} & \frac{\partial G_1}{\partial\dot{\theta}_n}\\ \frac{\partial G_2}{\partial\theta_n} & \frac{\partial G_2}{\partial\dot{\theta}_n}\end{bmatrix} \tag{3.2}$$

must always be greater than zero.

The value of J is simply related to the parameters of the differential equation, namely

$$J=e^{-(2\pi/\omega)/(\beta/\alpha)}\,, \tag{3.3}$$

so that $J<1$ (the map is area contracting) and independent of θ and $\dot{\theta}$ because of the simple choice of damping term in (2.1).[22]

If the motion is phase locked with

$$\langle\dot{\theta}\rangle=\frac{P}{Q}\omega\,,$$

it means that there exist periodic fixed points $(\theta^*,\dot{\theta}^*)$ such that

$$\underline{R}^Q\begin{bmatrix}\theta^*\\ \dot{\theta}^*\end{bmatrix}=\begin{bmatrix}\theta^*\\ \dot{\theta}^*\end{bmatrix}+\begin{bmatrix}2\pi P\\ 0\end{bmatrix}. \tag{3.4}$$

For small nonlinearity one expects that any motion will be either phase locked or quasiperiodic in which case the frequency, or winding number

$$W=\lim_{n\to\infty}(\theta_n/2\pi n)\,, \tag{3.5}$$

is irrational. The initial condition will soon be forgotten due to the damping of the motion. The mapping is area contracting and hence destroys information on the initial configuration, so the motion might asymptotically be confined to a smooth invariant curve $\theta(t)$ on the torus (Fig. 5). This means, of course, also that asymptotically $\dot{\theta}$ is just a given function of θ so that in terms of the map R there exists a smooth invariant curve

$$\dot{\theta}_n=g(\theta_n) \tag{3.6}$$

on which the asymptotic behavior takes place. Referring back to (3.1) and inserting (3.6), we find a unique relation

$$\theta_{n+1}=f(\theta_n)=G_1(\theta_n,g(\theta_n))\,, \tag{3.7}$$

where f is a circle map since it is periodic in θ_n. We shall denote this one-dimensional map the "reduced (return) map." In the following we shall assume that (3.6) and (3.7) are single-valued functions although all arguments below would hold just as well if they were just orientable curves.

Whether this dimensional reduction actually takes place depends crucially upon the assumption (3.6) for the ex-

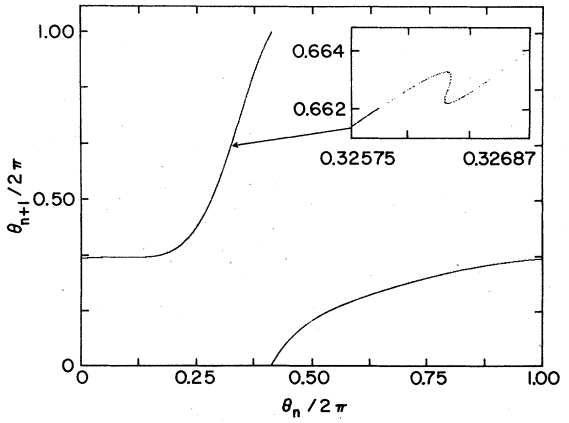

FIG. 9. Return map calculated for $\beta=1.253$, $A=1.2$; other parameters as in Fig. 8. The function develops a cubic inflection point indicating a transition to chaos. The inset shows an enlargement of the curve around $f^2(\theta_I)$ where θ_I is the inflection point $[f'(\theta_I)\sim 0, f^{2'}(\theta_I)\to\infty]$.

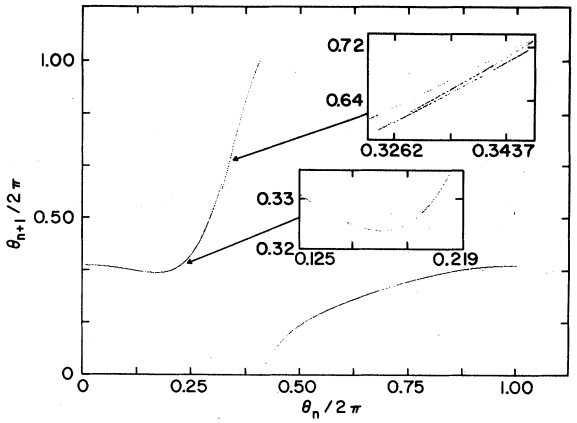

FIG. 10. Return map calculated for $\beta=1.081$, $A=1.094$. The map develops a local minimum and "wiggles" (insets) indicating chaotic behavior.

istence of an invariant curve, and for given values of the parameters we do not known whether or not it is satisfied (except in the limit $\alpha \ll 1$ where the connection with the circle map has been established analytically[18]). The best we can do is to generate (3.6) and (3.7) by solving the differential equation (2.1) numerically on the computer. Figure 8 shows the "reduced" map in a situation where this does indeed happen. The asymptotic form is quasiperiodic and the map is one dimensional (see inset). Changing some parameters (for instance, increasing A), we can generate plots that asymptotically display only a discrete set of points, namely the Q points $\theta_1^*,\theta_2^*,\ldots,\theta_Q^*$ (mod2π) which are the stable periodic points of the map R [or f in (3.7)]. The scenario is precisely the same as for the circle map studied in I. Increasing A still further leads again to quasiperiodic motion.

As described in I, chaotic motion in circle maps sets in when the map acquires zero slope somewhere in the interval, thus ceasing to be an invertible diffeomorphism. As long as the map is everywhere monotonic, erratic behavior can never occur.[3] Analogously, let us ask about the structure of the map f at the transition to chaos. Figures 8—10 show a sequence of reduced maps for winding numbers around $W\simeq 0.38$. In Fig. 8 the motion is regular, whereas Figs. 9 and 10 correspond to chaotic behavior. Superficially it appears that the map acquires a zero slope at the transition to chaos, so the transition would be described precisely as that occurring in a one-dimensional circle map.

However, as seen from Figs. 9 and 10 (especially the insets), the behavior of f around the transition point is more complicated: Instead of just turning over to form isolated local maxima and minima, the curve "crinkles up," and seems to be filled up in an uneven nonergodic way. In the next section we shall try to understand this behavior.

The most important observation made so far is that the return map is effectively one dimensional, up to and including the transition point. In Sec. V it will be argued that the critical behavior is indeed that of the circle map, despite the different features of the map near the transition.

IV. THE "CRITICAL LINE"

To study the region in which the reduced return map f approaches zero slope, we refer back to Eq. (3.1). Differentiating with respect to θ_n, using the assumption (3.6) of a smooth asymptotic orbit as well as the definition (3.7), we obtain

$$f'(\theta_n)=\frac{\partial G_1(\theta_n,g(\theta_n))}{\partial\theta_n}+g'(\theta_n)\frac{\partial G_1(\theta_n,g(\theta_n))}{\partial\dot{\theta}_n}\ , \tag{4.1a}$$

$$g'(\theta_{n+1})f'(\theta_n)=\frac{\partial G_2(\theta_n,g(\theta_n))}{\partial\theta_n}+g'(\theta_n)\frac{\partial G_2(\theta_n,g(\theta_n))}{\partial\dot{\theta}_n}\ . \tag{4.1b}$$

Now, if we focus our attention on a phase-locked state with winding number P/Q, the asymptotic motion really amounts to jumping between the Q different stable periodic points $\theta_1^*,\theta_2^*,\ldots,\theta_Q^*$ (mod2π), so the question arises whether $g'(\theta_n)$ has any meaning.

Quite generally, the map (3.1) is a map of the annulus. Figure 7 shows schematically the fixed-point structure for a periodic (phase-locked) state. In addition to the Q stable periodic points $(\theta_1^*,\dot{\theta}_1^*),\ldots,(\theta_Q^*,\dot{\theta}_Q^*)$, there are also Q unstable periodic points $(\theta_1^u,\dot{\theta}_1^u),\ldots,(\theta_Q^u,\dot{\theta}_Q^u)$. The unstable manifold of these unstable periodic points [i.e., the point set for which $R^{-n}(\bar{X})$ approaches the unstable periodic cycle as $n\to\infty$] is by definition the invariant circle of the map. The coordinates of this invariant circle are precisely $(\theta,g(\theta))$.

Having now given meaning to $g'(\theta)$ [and therefore to $f'(\theta)$], we shall see that a zero slope for $f(\theta)$ leads to trouble. Thus assume that

$$f'(\theta_n)=0\ . \tag{4.2}$$

Then it follows from (4.1a) and (4.1b) that

$$g'(\theta_{n+1})f'(\theta_n)\neq 0\ , \tag{4.3}$$

since the Jacobian (3.2) is never zero.

Now (4.3) implies that

$$|g'(\theta_{n+1})|\to\infty \tag{4.4}$$

if $f'(\theta_n)\to 0$. Using (4.1a) with $n\to n+1$, we find that

$$|f'(\theta_{n+1})|\to\infty \tag{4.5}$$

unless

$$\frac{\partial G_1(\theta_{n+1},g(\theta_{n+1}))}{\partial\dot{\theta}_{n+1}}=0\ . \tag{4.6}$$

Assuming that $f'(\theta_{n+1})$ remains finite, we must accept (4.6), and because the Jacobian is nonzero we obtain

$$\frac{\partial G_2(\theta_{n+1},g(\theta_{n+1}))}{\partial\dot{\theta}_{n+1}}\neq 0\ ; \tag{4.7}$$

therefore, from (4.1b) with $n\to n+1$

$$|g'(\theta_{n+2})f'(\theta_{n+1})|\to\infty \tag{4.8}$$

because of (4.4). Hence

$$|g'(\theta_{n+2})| \to \infty \ . \tag{4.9}$$

Iterating this argument we see that *in the generic case* $f'(\theta_n) \to 0$ *implies* $f(\theta_{n+1}) \to \infty$, as indicated numerically for the return map of the differential equation (2.1) (see Fig. 9). If the derivatives $\partial G_1(\theta_{n+j}, g(\theta_{n+j}))/\partial \dot{\theta}_{n+j}$ vanish for $j = 1, \ldots, N$ exceptionally, we will find that $f'(\theta_{n+1})$, $f'(\theta_{n+2}), \ldots, f'(\theta_{n+N})$ remain finite whereas $|f'(\theta_{n+N+1})| \to \infty$.

More precisely, we can follow the large terms in (4.1a) and (4.1b) as $f'(\theta_n) \to 0$. Assuming for simplicity that $\partial G_1/\partial \dot{\theta}$ never vanishes on the orbit, we find

$$f'(\theta_{n+1}) \sim -\frac{\left.\frac{\partial G_1}{\partial \dot{\theta}}\right|_{(\theta_{n+1}, g(\theta_{n+1}))}}{\left.\frac{\partial G_1}{\partial \dot{\theta}}\right|_{(\theta_n, g(\theta_n))}} \frac{J(\theta_n)}{f'(\theta_n)} \ . \tag{4.10}$$

Now J must always be positive. If, in addition, the derivatives of G_1 appearing in (4.10) have the same sign, the coefficient of $[f'(\theta_n)]^{-1}$ is negative. This is certainly true for a large class of two-dimensional maps showing phase locking and chaos, so we assume this to be "generically" true, i.e., only exceptionally violated.

If so, then (4.10) states that

$$f'(\theta_n) \to 0^+ \Longrightarrow f'(\theta_{n+1}) \to -\infty \ . \tag{4.11}$$

Consider now the graph of f as a function of a parameter and assume to start with that f is an increasing circle map. Varying the parameter decreases $f'(0)$ toward zero and by (4.11) $f'(f(0))$ must approach *minus infinity.* But then $f'(\theta)$ must be zero somewhere in the interval $[0, f(0)]$ giving another infinite slope, etc. The whole curve crinkles up as sketched in Figs. 11(a) and 11(b). Thus, the loss of monotonicity is tied to the loss of smoothness of the invariant circle: *If there exists a value of* θ *with* $f'(\theta) = 0$, *then the invariant circle has already broken up and the initial assumption of a smooth orbital* $g(\theta)$ *is contradictory.*[23]

There is one trivial way in which the curve might avoid crinkling up, namely if it forms a closed circuit. This means, however, that we have chosen the wrong variables: θ does not act as an angular variable and even for small nonlinearity there does not exist a single-valued $g(\theta)$ in (3.6).

A more interesting possibility is that the curve spirals as shown in Fig. 11(c). Here the analyticity is lost only in a finite number of points: the stable periodic points of the map. In this case the breakdown can be located by linear analysis of the map. To see this we return to (4.1a) and (4.1b), dividing (4.1a) with (4.1b). We then obtain an equation containing explicitly only g:

$$g'(\theta_{n+1}) = \frac{\partial G_2/\partial \theta_n + g'(\theta_n)\partial G_2/\partial \dot{\theta}_n}{\partial G_1/\partial \theta_n + g'(\theta_n)\partial G_1/\partial \dot{\theta}_n} \ . \tag{4.12a}$$

We now introduce functions $m(\theta)$ and $n(\theta)$ through

$$g'(\theta) = m(\theta)/n(\theta) \ , \tag{4.12b}$$

and rewrite (4.11a) as

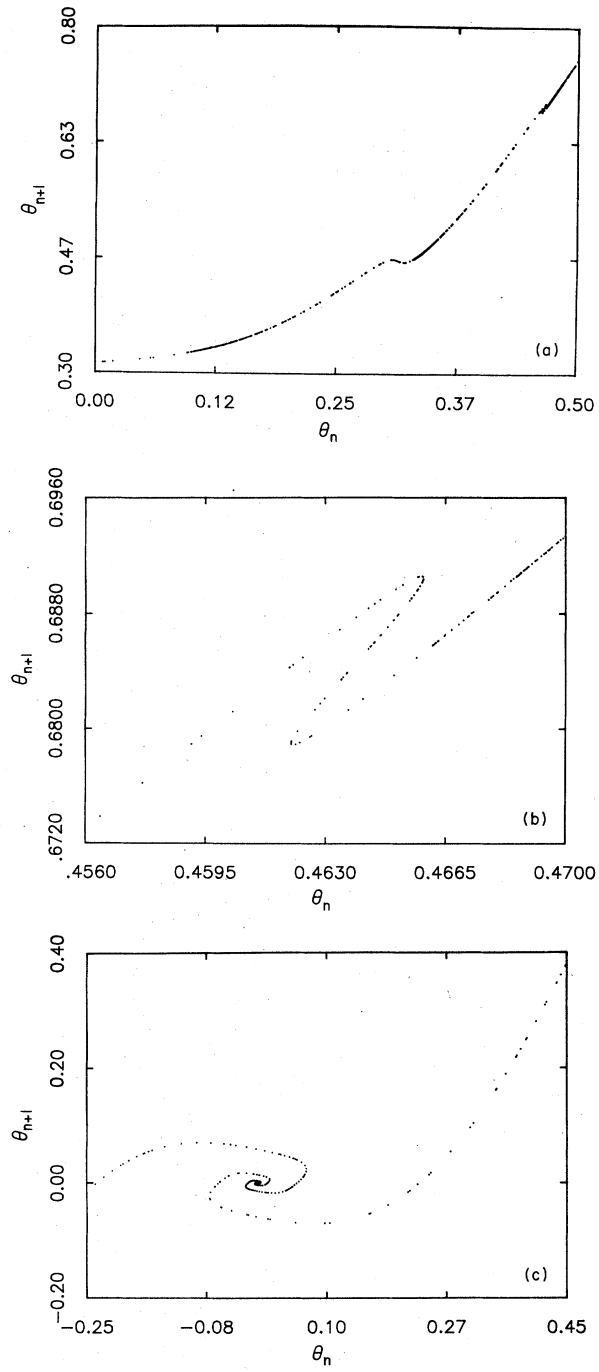

FIG. 11. Loss of smoothness of the invariant circle shown by different reduced return maps for the map (5.1) with $b = 0.25$. (a) The curve crinkles up close to criticality ($K = 1.1$, $\Omega = 0.292$). (b) Magnification of (a). (c) The map loses smoothness at the periodic point ($K = 1.25$, $\Omega = 0$).

$$\begin{bmatrix} n(\theta_{n+1}) \\ m(\theta_{n+1}) \end{bmatrix} = \underline{D}(\vec{\mathrm{X}}_n) \begin{bmatrix} n(\theta_n) \\ m(\theta_n) \end{bmatrix} \ , \tag{4.13}$$

where $\vec{\mathrm{X}}_n = (\theta_n, \dot{\theta}_n)$ and $\underline{D}$ is the Jacobian of the map (3.1). This defines n and m completely once they are specified at some initial point [for instance by $n(\theta_0) = 1$,

$m(\theta_0)=g'(\theta_0)$]. If the parameters are such that the map is periodic with winding number P/Q, the asymptotic behavior of (n,m) is given by

$$\begin{bmatrix} n(\theta_{n+Q}) \\ m(\theta_{n+Q}) \end{bmatrix} = \underline{D}(\vec{X}^*_Q)\underline{D}(\vec{X}^*_{Q-1})\cdots\underline{D}(\vec{X}^*_1)\begin{bmatrix} n(\theta_n) \\ m(\theta_n) \end{bmatrix} = \underline{M}(\vec{X}^*_Q,\ldots,\vec{X}^*_1)\begin{bmatrix} n(\theta_n) \\ m(\theta_n) \end{bmatrix}, \tag{4.14}$$

where θ_n and $\theta_{n+Q}=\theta^*_1 \pmod{2\pi}$.

Now $\underline{M}$ is a real matrix and has either two real eigenvalues $\lambda_1>\lambda_2$ or a complex conjugate pair. In the former case almost all initial choices $(n(\theta),m(\theta))$ will lead to

$$\begin{bmatrix} n(\theta_{n+NQ}) \\ m(\theta_{n+NQ}) \end{bmatrix} \to \lambda_1^N a\vec{e}_1 , \tag{4.15}$$

where $\vec{e}_1=(e_1^x,e_1^y)$ is the eigenvector of $\underline{M}$ corresponding to the largest eigenvalue and a is the projection,

$$a=(m(\theta_n),n(\theta_n))\cdot\vec{e}_1 . \tag{4.16}$$

Hence g' converges to the value

$$g'(\theta_{n+Q})=g'(\theta^*_1)=\frac{m(\theta_{n+Q})}{n(\theta_{n+Q})}\to\frac{e_1^y}{e_1^x} . \tag{4.17}$$

When the eigenvalues are complex conjugate pairs no simple asymptotic relation like (4.16) exists and $g'(\theta^*_1)$ becomes undefined. *The map loses its smoothness at the limit-cycle fixed point when the eigenvalues of the product of the "Jacobians" at the limit cycle points are identical,* $\lambda_1=\lambda_2=\sqrt{\det\underline{M}}$.[24]

In the next section we shall look at a particular two-dimensional dissipative map. Since we are looking for universal behavior we might as well choose a simple analytic map instead of doing cumbersome integration of the differential equation. For that particular map we shall try to locate the critical line, i.e., the line in parameter space where the smoothness breaks down.

The fundamental question is whether the critical line in any sense defines a smooth curve in parameter space. One might fear—since the condition of criticality at the periodic points relies upon properties of the matrix $\underline{M}$ defined in (4.13) and which explicitly depends upon Q, the denominator of the winding number—that the critical curve would be fundamentally fractal. Our finding—for the particular map which will be studied—is that it is not fractal: The dissipation present in the map secures that the critical line defined through the very high-order rational steps is smooth.

V. SCALING BEHAVIOR OF THE "DISSIPATIVE STANDARD MAP"

In this section we show numerical results for a particular two-dimensional map which could in principle be the return map of a second-order differential equation such as (2.1). The map is defined by recursion relations in two variables θ and r:

$$\begin{aligned} \theta_{n+1}&=\theta_n+\Omega-(K/2\pi)\sin(2\pi\theta_n)+br_n , \\ r_{n+1}&=br_n-(K/2\pi)\sin(2\pi\theta_n) , \end{aligned} \tag{5.1}$$

where b is between 0 and 1. The equation has the required symmetry in θ and the variable r_n plays a similar role as θ_n in (3.1). Note that we have inserted 2π's in the argument so that the map is periodic mod1.

The Jacobian matrix of the mapping is

$$\underline{D}=\begin{bmatrix} 1-K\cos(2\pi\theta) & b \\ -K\cos(2\pi\theta) & b \end{bmatrix} , \tag{5.2}$$

with $\det D=b$, showing that $b<1$ indeed defines an area contracting map corresponding to a dissipative dynamical system. When $b\to 0$ we recover the sine circle map (see I), and when $b\to 1$ we obtain the so-called standard area preserving map (Chirikov, Ref. 25).

In this case (4.10) reduces to

$$f'(\theta_{n+1})\sim -\frac{b}{f'(\theta_n)} \tag{5.3}$$

as $f'(\theta_n)\to 0$, so the conclusions below (4.10) are certainly valid in this case.

This map has been studied earlier both numerically[26] and by renormalization-group techniques[26,27] and it has been found that, for a series of winding numbers converging to the golden mean, $(\sqrt{5}-1)/2$, the scaling is the same as for one-dimensional circle maps. In the work by Rand *et al.*[27] the general structure of the locked steps was discussed on the basis of earlier findings (for a different map) by Aronson *et al.*[28] to which we shall return shortly.

As an illustrative example, let us consider the simplest phase-locked state, namely the one with winding number $W=0/1$. Here the map has two fixed points, one stable and one unstable. To find these we must solve the equations

$$\begin{aligned} \theta^*&=\theta^*+\Omega-\frac{K}{2\pi}\sin(2\pi\theta^*)+br^* , \\ r^*&=br^*-\frac{K}{2\pi}\sin(2\pi\theta^*) , \end{aligned} \tag{5.4}$$

giving

$$\begin{aligned} \sin(2\pi\theta^*)&=\frac{2\pi\Omega(1-b)}{K} , \\ r^*&=-\Omega , \end{aligned} \tag{5.5}$$

Indeed, (5.5) has either 0 or two solutions, the latter being the case when

$$|\Omega|<\Omega_e\equiv\frac{K}{2\pi(1-b)} . \tag{5.6}$$

The eigenvalues of the Jacobian matrix $\underline{D}$ are

$$\lambda=\tfrac{1}{2}(1+b-K\cos(2\pi\theta) \pm\{[1+b-K\cos(2\pi\theta)]^2-4b\}^{1/2}) \tag{5.7}$$

and the line confining the region where there exists a stable fixed point is found by solving

$$|\lambda|=1 . \tag{5.8}$$

Setting $\lambda=1$ gives us

$$\Omega=\pm\Omega_e \ , \tag{5.9}$$

but $\lambda=-1$ leads to a new hyperbolic constraint

$$\frac{K^2}{[2(1+b)]^2}-\frac{\Omega^2}{[2(1+b)/2\pi(1-b)]^2}=1 \ . \tag{5.10}$$

The criticality condition for the fixed point, $\lambda_1=\lambda_2$, can be written

$$1+b-K\cos(2\pi\theta^*)=\pm 2\sqrt{b} \ , \tag{5.11}$$

which depends on θ^*. Inserting (5.5) we can write it as

$$\frac{K^2}{(K_c^{\pm})^2}-\frac{\Omega^2}{[K_c^{\pm}/2\pi(1-b)]^2}=1 \ , \tag{5.12}$$

where

$$K_c^{\pm}=1+b\pm 2\sqrt{b}=(1\pm\sqrt{b})^2 \ . \tag{5.13}$$

The lower hyperbola (5.13) gives the maximum value of K for which f is smooth through the fixed point. Figure 12 shows one-half of the phase-locked region for $b=0.25$ (the other half is the mirror image). The curve through O and A' is the (lower) hyperbola and the straight line through A is the edge $\Omega=\Omega_e$. In order to locate the critical line we must know when other parts of the map f lose smoothness, i.e., at what parameters the more general crinkling up [Fig. 11(b)] takes place. As found by Aronson *et al.*[28] for a different map, and verified for our map by Rand *et al.*[27] this seems generically to happen on curves connecting the hyperbola with the edge of the Arnol'd tongue. The triangles in Fig. 12 are points on this curve intersecting the hyperbola at A'. The lowest part of the hyperbola (OA') thus actually represents the critical line, but further away from the center the critical line follows AA' (the triangles).

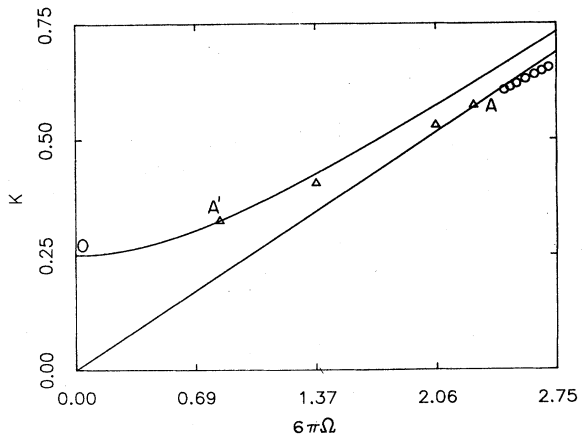

FIG. 12. Stability regime for fixed point with $W=0/1$ for $b=0.25$). Only one-half is shown since there is mirror symmetry around the y axis. The straight line through A is the edge $\Omega=\Omega_e$. The points marked by triangles indicate where the map crinkles up. The circles are tips of hyperbolas in the narrow locked regions just outside the edge. Note that the circles and triangles together seem to lie on a smooth curve cutting through the edge at A. This is strong evidence for the existence of a smooth critical line.

For higher-order locked steps the situation is similar, but we find that the point A' moves down towards O so that the critical line touches less of the hyperbola. Further, the whole line $OA'A$ becomes flatter: Due to the dissipation everything is squeezed together in a narrow K interval, rapidly decreasing with the order of the step. For high-order steps, the whole picture looks very much like the "skeleton" diagram for circle maps,[29] with "hyperbolas" just touching a smooth line.

For the general phase-locked step P/Q the analogs of (5.4), (5.8), and (5.11) cannot be solved analytically. If (θ_i,r_i), $i=1,\ldots,Q$ denote the Q stable periodic points, the stability condition for the step is that the eigenvalues of the matrix

$$\underline{M}=\prod_{i=1}^{Q}\underline{D}(\theta_i,r_i) \tag{5.14}$$

should have absolute value less than unity and the edges of the steps are found by solving

$$\lambda_{\max}=1 \tag{5.15a}$$

or

$$\mathrm{Tr}\underline{M}=1+b^Q \ . \tag{5.15b}$$

The Q-cycle fixed point becomes critical along a curve in (K,Ω) space where the eigenvalues of $\underline{M}$ are equal,

$$\lambda_1=\lambda_2=\sqrt{\det\underline{M}}=b^{Q/2} \tag{5.16a}$$

or

$$\mathrm{Tr}\underline{M}=2b^{Q/2} \ . \tag{5.16b}$$

This curve corresponds to the lower hyperbola for the 0/1 case (Fig. 12). In our numerical work we have taken the tip of the hyperbola (i.e., the analog of the point 0 in Fig. 12) simply as the point on the curve (5.16) with smallest K. Since the hyperbolas are generally tilted this is an approximation and we shall later explain how it can be improved. We have found these points numerically by a four-dimensional Newton iteration method (see Appendix) giving the values θ, r, Ω, and K at the tips of the hyperbolas for different P/Q. The resulting critical lines are shown in Figs. 1(a) and 1(b) for $b=0.25$ and in Fig. 1(c) for $b=0.5$, respectively.

The important finding is that even though the "curves" in Fig. 1 are wildly discontinuous at the low-order locked steps, *they seem to approach smoothness very quickly as the order Q of the resonance increases.* Thus on each edge of a given rational step there is a unique accumulation point for the tips of hyperbolas coming from very-high-order rationals converging to the given one, and if a smooth critical curve really exists, *these points are precisely the endpoints (denoted by A in Fig. 12) of the critical curve within the step.* This is shown clearly in Fig. 12 where the circles in the right-hand corner are the tips of high-order hyperbolas close to the locked region. They accumulate to the same point A and seem to form a smooth curve together with the triangles. Thus one can imagine the critical line extending outside of the step in Fig. 12, i.e., beyond A, where the invariant circle (in some very-high-

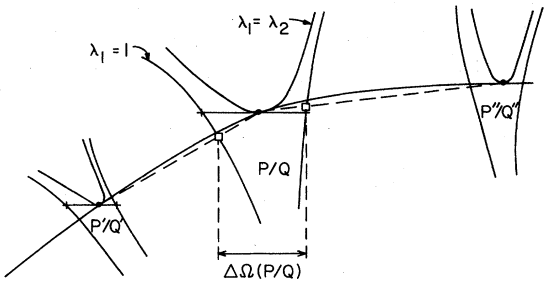

FIG. 13. Schematic diagram showing the hyperbolas where the invariant circle becomes critical through the stable periodic points, and the "true" critical curve. The squares, and the + 's represent the edges of the P/Q steps at criticality as estimated using the numerical methods presented here. The superstable point where the hyperbola touches the stability curve is approximated by the minimum point ●.

order steps) crinkles up. By emphasizing only the behavior within a single Arnol'd tongue, earlier treatments[27,28] have failed to make this clear.

Our conclusion is then that *there exists a smooth limiting critical line on which the invariant circles with irrational winding numbers break down.* Since our primary aim is to study the metric properties of the parameter values corresponding to irrational winding numbers on the critical line (i.e., the complement of the locked steps), we can continue this line through rational steps in any smooth way for calculational purposes. On crossing the critical line the reduced map loses monotonicity as shown in Figs. 11(a) and 11(b) (for $b=0.25$). The crinkling shown here is very much like the behavior seen in Figs. 9 and 10 for the "Josephson map" (although the damping in the latter case was much larger).

We can now return to the approximation made in locating the tips of the hyperbolas. Since we now conjecture that the "limit curve" is smooth (Fig. 1), we should actually locate them as the touching points of the envelope for the hyperbolas as shown in Fig. 13. For more accurate calculations this should be taken into account.

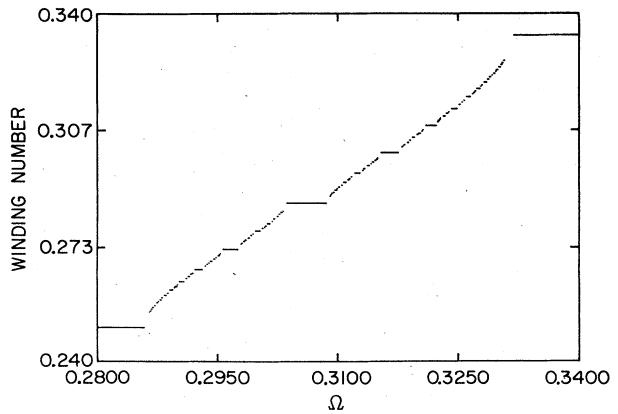

FIG. 14. Winding number P/Q vs Ω at criticality for the map (5.1) with $b=0.25$. Note the self-similar structure of the staircase as for the circle map (see I).

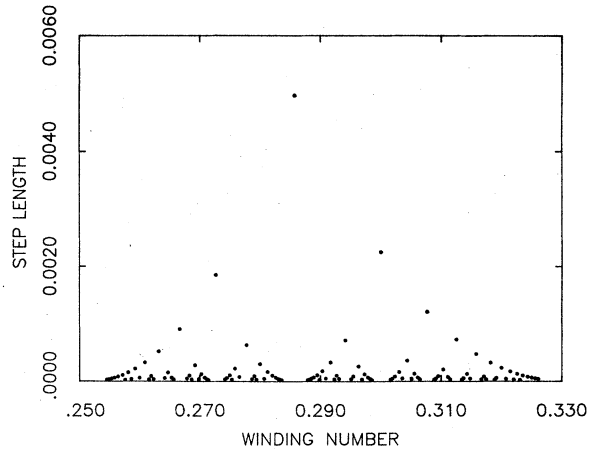

FIG. 15. The widths of phase-locked steps at criticality for the map (5.1) with $b=0.25$. Note the similarity with the circle map (see I).

Having argued for the existence of a smooth critical line we may address the question of possible scaling behavior along this line as found for one-dimensional

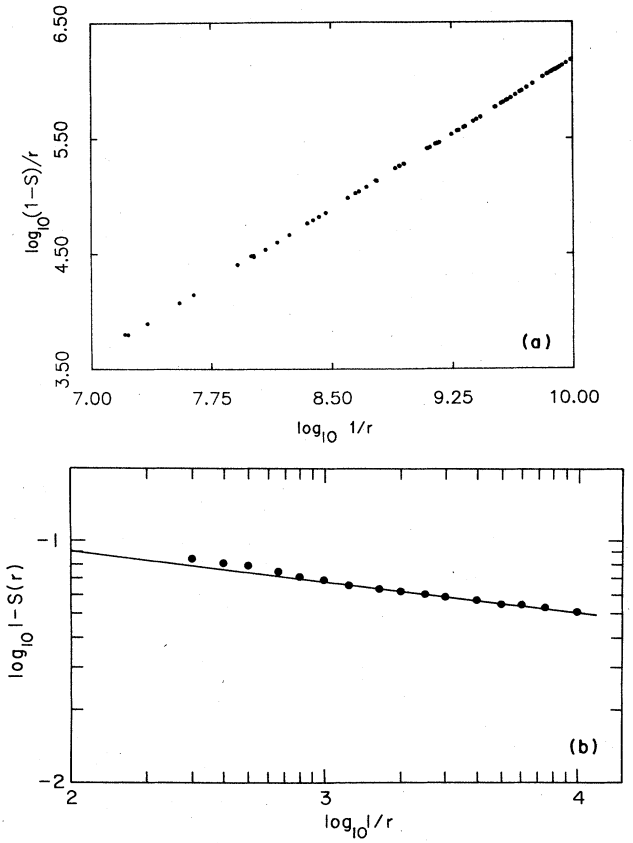

FIG. 16. Number of holes, $[1-S(r)]/r$ plotted vs r at criticality for the standard map (5.1). The linear behavior indicates that the staircase is complete. The critical index D (the fractal dimension of the staircase) was estimated from the slope. (a) $b=0.25$, $\frac{1}{4} < W < \frac{1}{3}$; $D=0.86\pm0.01$. (b) $b=0.5$, $\frac{1}{2} < W < \frac{2}{3}$; $D=0.87\pm0.01$.

maps (I). To find the endpoints of the P/Q steps we use the critical line defined by the highest-order steps. This was done for $b=0.25$, $\frac{1}{4} \leq W \leq \frac{1}{3}$ and for $b=0.5$, $\frac{1}{2} \leq W \leq \frac{2}{3}$; in both cases approximately 100 steps were found. For $b=0.25$ the edge was found by moving along a critical line defined by linear interpolation between the approximate accumulation points on the edges (the points marked by squares in Fig. 13), whereas the edge points for $b=0.5$ simply have K equal to the K values of the corresponding accumulation points (the points marked by plus in Fig. 13). In the limit the two methods are, of course, identical. For a given rational step the projection of the endpoints to the Ω axis determines $\Delta\Omega(P/Q)$—the width of the step. Figure 14 shows the winding number versus Ω on the critical line (for b=0.25)—the "devil's staircase" similar to the diagram (I, Fig. 3) for the circle map. Figure 15 shows the widths of the steps $\Delta(P/Q)$ plotted versus $W=P/Q$; the self-similar structure is quite apparent and the similarity with (I, Fig. 5) for the circle map is striking. Figure 16(a) and 16(b) shows the "number of holes" $[1-S(r)]/r$ plotted versus r as for the circle map, where $S(r)$ is the total width of steps which are wider than r. The plot in Fig. 16(a) is for $b=0.25$; the plot in Fig. 16(b) is for $b=0.5$. The linear behavior indicates scaling behavior at criticality. The slope of the straight line yields

$$[1-S(r)]/r \sim r^{D} \tag{5.17}$$

with $D \sim 0.86 \pm 0.01$. Hence, the staircase is complete, and the fractal dimension of the staircase, or the complementary Cantor set is $D \sim 0.86$. The accuracy of this estimate is much less than the one for the circle map in I since (i) a much smaller number of steps were used to estimate D and (ii) there is additional uncertainty related to the estimate of the critical curve, which was given simply by $K=1$ in the circle-map case. Within the uncertainty, the critical behavior for the standard map is the same as for the circle map.

VI. CONCLUSION

In papers I and II we have investigated the transition to chaos caused by overlap of resonances by studying circle maps, differential equations representing actual physical systems, and 2D dissipative maps. Our conjecture is that the critical behavior of all these systems is the same, namely that of the circle map. We urge that experiments on Josephson junctions, charge-density-wave systems, and other systems with two competing periodicities be performed to check our predictions.

We are aware of three experiments which have been performed since we first announced our results: Kao *et al.*[30] and Alstrom *et al.*[31] have studied the differential equation (5.1) with a "Josephson junction simulator;" they find scaling behavior as predicted here, with $D \sim 0.91 \pm 0.04$ and $D \sim 0.87 \pm 0.02$, respectively. More importantly, Brown, Mozurkewich, and Grüner[21] have measured subharmonic steps in the CDW system $NbSe_3$ in ac plus dc electric fields; they also find scaling behavior in agreement with our conjecture, with $D \sim 0.91 \pm 0.03$. We feel that the accuracy of the experiments could be improved; in particular, more work should be done to locate the critical line, following, for instance, the ideas presented here. It would be of interest to measure the return map directly. The most precise measurements can probably be performed on Josephson junctions in microwave fields, but no experiment on the scaling behavior near the critical point has been reported so far.

ACKNOWLEDGMENTS

We have enjoyed many helpful discussions with our colleagues on the subject of this article. It is a pleasure to thank especially Mitchell Feigenbaum, Michael Fisher, George Grüner, Phil Holmes, Yittan Kao, Mogens Levinsen, David Rand, John Sampson, Scott Shenker, Eric Siggia, and Gertrud Zwicknagel. We are grateful to K. Fesser, A. Bishop, and P. Kumar for discussions on the possibility of having one-dimensional return maps for higher-dimensional systems. One of us (M.H.J.) is grateful to Brookhaven National Laboratory for kind hospitality. Another one of us (T.B.) would like to acknowledge support by National Science Foundation Grant No. DMR-83-14625. The work at Brookhaven National Laboratory was supported by The Division of Material Sciences of the U.S. Department of Energy under Contract No. DE-AC02.76CH00016.

APPENDIX: NUMERICAL PROCEDURES FOR DETERMINING CRITICAL LINE AND STEP WIDTHS

The critical points, indicated by ● in Fig. 14, fulfill the fixed point conditions:

$$g_1=\theta_n-\theta_0-P=0\,, \tag{A1}$$

$$g_2=r_n-r_0=0\,, \tag{A2}$$

and the criticality condition,

$$g_3=\mathrm{Tr}\underline{M}(\theta_0,r_0)=\mathrm{Tr}\prod_i \underline{D}(\theta_i,r_i)=2b^{Q/2}\,. \tag{A3}$$

The fourth condition is that $\mathrm{Tr}\underline{M}$ be a minimum subject to the constraints (A1) and (A2) for a given K.

Using Lagrange-multiplier technique, we form the function

$$F=g_3-L_1g_1-L_2g_2\,, \tag{A4}$$

where L_1 and L_2 are Lagrange multipliers. The constrained minimum condition can be expressed as

$$\begin{aligned}
\frac{\partial F}{\partial\theta_0}&=\frac{\partial g_3}{\partial\theta_0}-L_1\frac{\partial g_1}{\partial\theta_0}-L_2\frac{\partial g_2}{\partial\theta_0}\,,\\
\frac{\partial F}{\partial r_0}&=\frac{\partial g_3}{\partial r_0}-L_1\frac{\partial g_1}{\partial r_0}-L_2\frac{\partial g_2}{\partial r_0}\,,\\
\frac{\partial F}{\partial\Omega}&=\frac{\partial g_3}{\partial\Omega}-L_1\frac{\partial g_1}{\partial\Omega}-L_2\frac{\partial g_2}{\partial\Omega}\,.
\end{aligned} \tag{A5}$$

This system of equations has solutions for L_1 and L_2 only if its determinant is zero:

$$H=\begin{vmatrix} \frac{\partial g_1}{\partial\theta_0} & \frac{\partial g_2}{\partial\theta_0} & \frac{\partial g_3}{\partial\theta_0} \\ \frac{\partial g_1}{\partial r_0} & \frac{\partial g_2}{\partial r_0} & \frac{\partial g_3}{\partial r_0} \\ \frac{\partial g_1}{\partial\Omega} & \frac{\partial g_2}{\partial\Omega} & \frac{\partial g_3}{\partial\Omega} \end{vmatrix}=0\ . \tag{A6}$$

Hence, the fourth condition is

$$g_4=H=0\ .$$

The critical point is the point where the parameters θ_0, r_0, Ω, and K fulfil the conditions (A1), (A2), (A3), and (A6). This point is found by means of a four-dimensional Newton iteration method as described in I.

The end points of the limit cycle steps are found by a similar Newton iteration method. The parameters θ_0, r_0, and Ω must fulfil the fixed-point conditions (A1) and (A2) in addition to the stability condition

$$g_3=\mathrm{Tr}\underline{M}(\theta_0,r_0)=1+b^{Q}\ . \tag{A7}$$

In all cases the quantities $\partial g_i/\partial\theta_0$, etc. (which involves derivatives up to third order) can be found recursively as described in I.

[1]Stated in a footnote in B. van der Pol, Philos. Mag. 3, 13 (1927). We thank David Rand for making us aware of this.

[2]P. Bak, T. Bohr, M. H. Jensen, and P. V. Christiansen, Solid State Commun. **51**, 231 (1984).

[3]V. I. Arnol'd, Am. Math. Soc. Trans., Ser. 2, **46**, 213 (1965); M. R. Herman, in *Geometry and Topology,* edited by J. Palis (Springer, Berlin, 1979), Vol. 579, p. 271.

[4]J. Moser, *Stable and Random Motions in Dynamical Systems* (Princeton University Press, Princeton, 1973).

[5]For reviews, see P. E. Lindelof, Rep. Prog. Phys. **44**, 949 (1981); Y. Imry, in *Statics and Dynamics of Nonlinear Systems,* edited by G. Benedek, H. Bilz, and R. Zeyher (Springer, Berlin, 1983), p. 170.

[6]R. Y. Chiao, M. J. Feldman, D. W. Peterson, B. A. Tucker, and M. T. Levinsen, in *Future Trends in Superconducting Electronics (Charlottesville, 1978),* proceedings of the Conference on the Future Trends in Superconductive Electronics, edited by B. S. Deaver, C. M. Falco, J. H. Harris, and S. A. Wolf (AIP, New York, 1979). p. 259.

[7]V. N. Belykh, N. F. Pedersen, and O. H. Soerensen, Phys. Rev. B **16**, 4860 (1978).

[8]Y. Braiman, E. Ben-Jacob, and Y. Imry, in *SQUID 80,* edited by H. D. Hahlbohm and H. Lubbig (de Gruyter, Berlin, 1980); E. Ben-Jacob, Y. Braiman, R. Shansky, and Y. Imry, Appl. Phys. Lett. **38**, 822 (1981); E. Ben-Jacob, I. Goldhirsch, Y. Imry, and S. Fishman, Phys. Rev. Lett. **49**, 1599 (1982); R. L. Kautz, J. Appl. Phys. **52**, 6241 (1981).

[9]B. A. Huberman, J. P. Crutchfield, and N. H. Packard, Appl. Phys. Lett. **37**, 751 (1980); D. D'Humieres, M. R. Beasley, B. A. Huberman, and A. Libchaber, Phys. Rev. A **26**, 3483 (1982); N. F. Pedersen and A. Davidson, Appl. Phys. Lett. **39**, 830 (1981); M. Cirillo and N. F. Pedersen, Phys. Lett. **90A**, 150 (1982); W. J. Yeh and Y. H. Kao, Phys. Rev. Lett. **49**, 1888 (1982); A. H. MacDonald and M. Plischke, Phys. Rev. B **27**, 201 (1983). W. J. Yeh and Y. H. Kao, Appl. Phys. Lett. **42**, 299 (1983). These papers deal with the case $A=0$, which is less relevant here.

[10]M. T. Levinsen, J. Appl. Phys. **53**, 4294 (1982).

[11]F. M. A. Salam and S. S. Sastry (unpublished).

[12]G. Grüner, A. Zawadowski, and P. M. Chaikin, Phys. Rev. Lett. **46**, 511 (1981); J. Bardeen, E. Ben-Jacob, A. Zettl, and G. Grüner, Phys. Rev. Lett. **49**, 493 (1982).

[13]A. Zettl and G. Grüner, Solid State Commun. **46**, 501 (1983); Phys. Rev. B **29**, 755 (1984).

[14]P. Monceau, J. Richard, and M. Renard, Phys. Rev. Lett. **45**, 43 (1980); Phys. Rev. B **25**, 931 (1982).

[15]P. Bak, Rep. Prog. Theor. Phys. **45**, 587 (1982).

[16]W. C. Stewart, Appl. Phys. Lett. **12**, 277 (1981); D. E. McCumber, J. Appl. Phys. **39**, 3113 (1968).

[17]M. J. Renne and D. Polder, Rev. Phys. Appl. **9**, 25 (1974); J. R. Waldram and P. H. Wu, J. Low Temp. Phys. **47**, 363 (1982).

[18]M. Ya. Azbel and P. Bak, Phys. Rev. B (to be published).

[19]S. Shapiro, Phys. Rev. Lett. **11**, 80 (1963).

[20]Although workers in the field using Josephson junctions as measuring devices would prefer to get rid of the subharmonic steps as well as the noise.

[21]S. E. Brown, G. Mozurkewich, and G. Grüner, Phys. Rev. Lett. **54**, 2272 (1984).

[22]For a general method of computing J see, e.g., M. L. Cartwright, in *Contributions to the Theory of Nonlinear Oscillations,* Vol. 20 of *Annals of Mathematics Studies* (Princeton University, Princeton, N.J., 1950), p. 149.

[23]A consequence of this is that the return map of a second-order differential equation cannot be a simple 1D logistic map with a local maximum. At best, a 1D map is a good approximation to the 2D map.

[24]For a different argument leading to this criterion, see Ref. 28.

[25]B. V. Chirikov, Phys. Rep. **52**, 263 (1979).

[26]M. J. Feigenbaum, L. P. Kadanoff, and S. J. Shenker, Physica (Utrecht) **5D**, 370 (1982).

[27]D. Rand, S. Ostlund, J. Sethna, and E. Siggia, Phys. Rev. Lett. **49**, 132 (1982); Physica (Utrecht) **6D**, 303 (1984).

[28]D. G. Aronson, M. A. Chory, G. R. Hall, and R. P. McGehee, Commun. Math. Phys. **83**, 303 (1982).

[29]L. Glass and R. Perez, Phys. Rev. Lett. **48**, 1772 (1982).

[30]W. J. Yeh, Da-Ren He, and Y. H. Kao, Phys. Rev. Lett. **52**, 480 (1984).

[31]P. Alstrom, M. T. Levinsen, and M. H. Jensen, Phys. Lett. **103A**, 171 (1984).